INTERNATIONAL JOURNAL FOR NUMERICAL METHODS IN FLUIDS, VOL. 17, 257–270 (1993)

NUMERICAL STUDY ON THE TWO-PHASE FLOW DISTRIBUTION IN A T-JUNCTION

L. F. M. MOURA* AND K. S. REZKALLAH

Mechanical Engineering Department, University of Saskatchewan, Saskatoon, SK, S7N 0W0, Canada

SUMMARY

The main objective of this paper is to investigate the ability of a two-dimensional two-fluid computer code to predict the phase separation in a T-junction. A new semi-implicit numerical scheme is developed for solving the two-fluid model equations. Special attention is directed to the modelling of the constitutive equations for the interfacial friction term. Detailed distribution of void fraction, pressure and velocities are obtained for an air–water mixture in a vertical tee. Good agreement was obtained between the computer code results and the experimental data for the phase separation in the T-junction.

KEY WORDS Two-phase flow Phase separation Two-fluid model Numerical simulation T-junction

INTRODUCTION

The two-phase gas–liquid flow distribution in a T-junction and other branching geometries has many industrial applications such as the petroleum industry, chemical process plants, power plants and water cooled nuclear reactors. The problem can briefly be stated as follows: if the flow conditions (total mass flow rate and gas quality) are known at the inlet tube, there is no general method to calculate the flow conditions in the main outlet tube or in the branch tube.

A literature survey showed that several investigations have been undertaken in T-junction two-phase flow during the past 10 years. The most recent experimental and analytical investigations[1–9] showed that the two phases are generally distributed unequally among the outlets, but the manner in which the phases are distributed is not yet well understood.

Considerable advances have been made in the last 20 years in the modelling of vapour–liquid two-phase flows.[10] Among these models, the most accurate one is that which is based on a two-fluid model approach. In such a model, the conservation equations for each phase are used in conjunction with some appropriate constitutive relations.[11] Several methods have been proposed for solving the two-fluid model equations.[12] They mainly differ in the degree of implicity which is used (from explicit to fully implicit schemes), and in the numerical procedure used for solving the velocity–pressure coupling.

In this paper a new semi-implicit scheme for solving the two-fluid model equations is presented. All terms in the momentum equation are calculated implicitly except for the convective term which is calculated explicitly. The transport properties are evaluated by using a donor-cell scheme. The conservation equations are reduced to an elliptic pressure problem. This procedure

* Mechanical Engineering Department, University of Campinas, Campinas 13081, Brazil.

0271–2091/93/150257–14$12.00

Received 12 September 1991
Revised 7 January 1993

is doubly advantageous since the number of unknowns is sharply reduced, and the reduced problem is a familiar one for which a number of powerful methods are available. Once the pressure values are obtained, the other unknowns are determinated from them. The resulting Newton iteration converges after a few trials.

It is well known that the constitutive equations for the interfacial terms are the weakest link in a two-fluid model. Unfortunately, to-date there is no general formulation for these equations. The interfacial momentum transfer has been successfully modelled for dispersed two-phase flows.[11] In this work an interfacial friction model is developed in order to cover the complete range of void fractions that may exist in the vicinity of the T-junction.

The purpose of this paper is to investigate the ability of a newly developed two-dimensional, two-phase flow computer code to predict the phase separation for an air–water mixture flowing in a vertical T-junction.

TWO-FLUID MODEL

The two-fluid model has been obtained by using temporal or statistical averaging.[13] The model is expressed in terms of two sets of conservation equations governing the balance of mass, momentum and energy in each phase. However, since the averaged fields of one phase are not independent of the other phase, the interaction terms which couple the transport of mass, momentum and energy of each phase across the interface appear in the field equations as source terms.

For the numerical study of the two-phase flow in a T-junction some simplifications may be formulated. The flow is supposed to be isothermal with no mass transfer. In addition, the viscous and the turbulent diffusion processes are neglected. These simplifications are possible because of the short length of the T-junction. Then, for a two-dimensional flow in the x–z plane, the two-fluid model conservation equations become

$$\frac{\partial}{\partial t}(\alpha_\ell \rho_\ell)+\frac{\partial}{\partial x}(\alpha_\ell \rho_\ell u_\ell)+\frac{\partial}{\partial z}(\alpha_\ell \rho_\ell w_\ell)=0, \tag{1}$$

$$\frac{\partial}{\partial t}(\alpha_g \rho_g)+\frac{\partial}{\partial x}(\alpha_g \rho_g u_g)+\frac{\partial}{\partial z}(\alpha_g \rho_g w_g)=0, \tag{2}$$

$$\frac{\partial}{\partial t}(\alpha_\ell \rho_\ell u_\ell)+\frac{\partial}{\partial x}(\alpha_\ell \rho_\ell u_\ell^2)+\frac{\partial}{\partial z}(\alpha_\ell \rho_\ell u_\ell w_\ell)=-\alpha_\ell \frac{\partial P}{\partial x}+\alpha_\ell \rho_\ell g_x+K_{g\ell}(u_g-u_\ell), \tag{3}$$

$$\frac{\partial}{\partial t}(\alpha_\ell \rho_\ell w_\ell)+\frac{\partial}{\partial x}(\alpha_\ell \rho_\ell u_\ell w_\ell)+\frac{\partial}{\partial z}(\alpha_\ell \rho_\ell w_\ell^2)=-\alpha_\ell \frac{\partial P}{\partial z}+\alpha_\ell \rho_\ell g_z+K_{g\ell}(w_g-w_\ell), \tag{4}$$

$$\frac{\partial}{\partial t}(\alpha_g \rho_g u_g)+\frac{\partial}{\partial x}(\alpha_g \rho_g u_g^2)+\frac{\partial}{\partial z}(\alpha_g \rho_g u_g w_g)=-\alpha_g \frac{\partial P}{\partial x}+\alpha_g \rho_g g_x+K_{g\ell}(u_\ell-u_g), \tag{5}$$

$$\frac{\partial}{\partial t}(\alpha_g \rho_g w_g)+\frac{\partial}{\partial x}(\alpha_g \rho_g u_g w_g)+\frac{\partial}{\partial z}(\alpha_g \rho_g w_g^2)=-\alpha_g \frac{\partial P}{\partial z}+\alpha_g \rho_g g_z+K_{g\ell}(w_\ell-w_g), \tag{6}$$

where ℓ stands for liquid and g for gas, u the velocity in the x direction, w the velocity in the z direction, α the volumetric fraction, ρ the density, P the pressure, g_x the gravity in x direction, g_z the gravity in z direction and $K_{g\ell}$ is the interfacial friction coefficient.

We have six differential equations and nine dependent variables:

$$\alpha_\ell, \alpha_g, \rho_\ell, \rho_g, u_\ell, u_g, w_\ell, w_g \text{ and } P.$$

To complete the equation set, we use the following relation:

$$\alpha_\ell + \alpha_g = 1, \tag{7}$$

$$\rho_\ell = f(P), \tag{8}$$

$$\rho_g = f(P). \tag{9}$$

Usually, the liquid is supposed to be incompressible. The ideal gas state equation may be used for the vapour phase.

To solve this set of equations we need a constitutive equation for the interfacial friction coefficient $K_{g\ell}$.

NUMERICAL METHOD

The conservation equations are discretized by using the finite volume technique and the staggered grid concept.[14] A detailed description of the numerical method is given elsewhere;[15] then only the main steps will be developed below.

The momentum equations are rewritten in a non-conservative form. The liquid mass conservation equation (1) is multiplied by the velocity in the x and z directions:

$$u_\ell \frac{\partial}{\partial t}(\alpha_\ell \rho_\ell) + u_\ell \frac{\partial}{\partial x}(\alpha_\ell \rho_\ell u_\ell) + u_\ell \frac{\partial}{\partial z}(\alpha_\ell \rho_\ell w_\ell) = 0, \tag{10}$$

$$w_\ell \frac{\partial}{\partial t}(\alpha_\ell \rho_\ell) + w_\ell \frac{\partial}{\partial x}(\alpha_\ell \rho_\ell u_\ell) + w_\ell \frac{\partial}{\partial z}(\alpha_\ell \rho_\ell w_\ell) = 0. \tag{11}$$

Now, these equations are subtracted from the liquid momentum equation in the x *and* z directions (3, 4):

$$\alpha_\ell \rho_\ell \frac{\partial}{\partial t} u_\ell + \alpha_\ell \rho_\ell u_\ell \frac{\partial}{\partial x} u_\ell + \alpha_\ell \rho_\ell w_\ell \frac{\partial}{\partial z} u_\ell + \alpha_\ell \frac{\partial P}{\partial x} = \alpha_\ell \rho_\ell g_x + K_{g\ell}(u_g - u_\ell), \tag{12}$$

$$\alpha_\ell \rho_\ell \frac{\partial}{\partial t} w_\ell + \alpha_\ell \rho_\ell u_\ell \frac{\partial}{\partial x} w_\ell + \alpha_\ell \rho_\ell w_\ell \frac{\partial}{\partial z} w_\ell + \alpha_\ell \frac{\partial P}{\partial z} = \alpha_\ell \rho_\ell g_z + K_{g\ell}(w_g - w_\ell). \tag{13}$$

In the same way, the gas mass conservation equation (2) is multiplied by the gas velocity in the x and z directions:

$$u_g \frac{\partial}{\partial t}(\alpha_g \rho_g) + u_g \frac{\partial}{\partial x}(\alpha_g \rho_g u_g) + u_g \frac{\partial}{\partial z}(\alpha_g \rho_g w_g) = 0, \tag{14}$$

$$w_g \frac{\partial}{\partial t}(\alpha_g \rho_g) + w_g \frac{\partial}{\partial x}(\alpha_g \rho_g u_g) + w_g \frac{\partial}{\partial z}(\alpha_g \rho_g w_g) = 0 \tag{15}$$

and subtracted from the gas momentum equation in the x (5) and z directions (6):

$$\alpha_g \rho_g \frac{\partial}{\partial t} u_g + \alpha_g \rho_g u_g \frac{\partial}{\partial x} u_g + \alpha_g \rho_g w_g \frac{\partial}{\partial z} u_g + \alpha_g \frac{\partial P}{\partial x} = \alpha_g \rho_g g_x + K_{g\ell}(u_\ell - u_g), \tag{16}$$

$$\alpha_g \rho_g \frac{\partial}{\partial t} w_g + \alpha_g \rho_g u_g \frac{\partial}{\partial x} w_g + \alpha_g \rho_g w_g \frac{\partial}{\partial z} w_g + \alpha_g \frac{\partial P}{\partial z} = \alpha_g \rho_g g_z + K_{g\ell}(w_\ell - w_g). \tag{17}$$

The liquid and gas mass conservation equations (1) and (2) are integrated over the volume $\mathrm{Vol}^{\mathrm{m}}$ shown in Figure 1:

$$\frac{\mathrm{Vol}^{\mathrm{m}}}{\Delta t}[(\alpha_\ell \rho_\ell)^{n+1}-(\alpha_\ell \rho_\ell)^n]+[A\alpha_\ell \rho_\ell u_\ell]_{\mathrm{W}}^{\mathrm{E}}+[A\alpha_\ell \rho_\ell w_\ell]_{\mathrm{S}}^{\mathrm{N}}=0, \tag{18}$$

$$\frac{\mathrm{Vol}^{\mathrm{m}}}{\Delta t}[(\alpha_{\mathrm{g}} \rho_{\mathrm{g}})^{n+1}-(\alpha_{\mathrm{g}} \rho_{\mathrm{g}})^n]+[A\alpha_{\mathrm{g}} \rho_{\mathrm{g}} u_{\mathrm{g}}]_{\mathrm{W}}^{\mathrm{E}}+[A\alpha_{\mathrm{g}} \rho_{\mathrm{g}} w_{\mathrm{g}}]_{\mathrm{S}}^{\mathrm{N}}=0, \tag{19}$$

where, $n+1$ is the value calculated in the actual time step, n the value calculated in the old time step, A the area of the volume face and E, W, N, S denote east, west, north and south cell faces.

The value of the scalar variables on the volume faces are calculated by using the donor-cell scheme.

The liquid momentum equation (12) in the x direction is integrated over the volume Vol^x shown in Figure 2:

$$\mathrm{Vol}^x\left[(\alpha_\ell \rho_\ell)^n \frac{u_{\ell i,k}^{n+1}-u_{\ell i,k}^n}{\Delta t}+\alpha_\ell^n \frac{P_{i,k}^{n+1}-P_{i-1,k}^{n+1}}{\Delta x}-K_{\mathrm{g}\ell}^n(u_{\mathrm{g}i,k}^{n+1}-u_{\ell i,k}^{n+1})\right]$$
$$+\int_{\mathrm{Vol}^x} \mathrm{C}\cdot u_\ell \,\mathrm{d}V=\mathrm{Vol}^x(\alpha_\ell \rho_\ell)^n g_x, \tag{20}$$

where $\mathrm{C}\cdot u_\ell$ represents the convective transport of u_ℓ.

Equation (20) may be rewritten in explicit form for the liquid velocity in the x direction:

$$d_\ell^x u_{\ell i,k}^{n+1}=a_\ell^x(P_{i,k}^{n+1}-P_{i-1,k}^{n+1})+b_\ell^x u_{\mathrm{g}i,k}^{n+1}+c_\ell^x. \tag{21}$$

In the same way, the gas momentum equation (14) in the x direction is integrated over the volume Vol^x shown in Figure 2:

$$\mathrm{Vol}^x\left[(\alpha_{\mathrm{g}} \rho_{\mathrm{g}})^n \frac{u_{\mathrm{g}i,k}^{n+1}-u_{\mathrm{g}i,k}^n}{\Delta t}+\alpha_{\mathrm{g}}^n \frac{P_{i,k}^{n+1}-P_{i-1,k}^{n+1}}{\Delta x}-K_{\mathrm{g}\ell}^n(u_{\ell i,k}^{n+1}-u_{\mathrm{g}i,k}^{n+1})\right]$$
$$+\int_{\mathrm{Vol}^x} \mathrm{C}\cdot u_{\mathrm{g}} \,\mathrm{d}V=\mathrm{Vol}^x(\alpha_{\mathrm{g}} \rho_{\mathrm{g}})^n g_x, \tag{22}$$

Therefore,

$$d_{\mathrm{g}}^x u_{\mathrm{g}i,k}^{n+1}=a_{\mathrm{g}}^x(P_{i,k}^{n+1}-P_{i-1,k}^{n+1})+b_{\mathrm{g}}^x u_{\ell i,k}^{n+1}+c_{\mathrm{g}}^x. \tag{23}$$

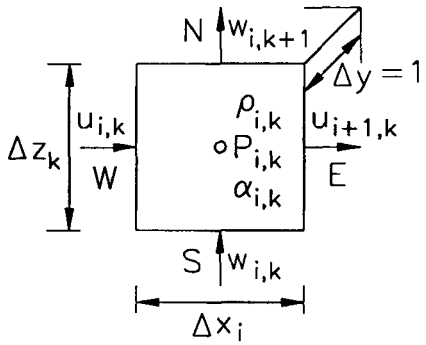

Figure 1. Volume $\mathrm{Vol}^{\mathrm{m}}$—mass conservation equation

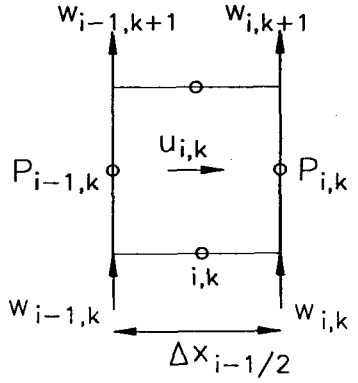

Figure 2. Volume Vol^x—momentum equation in the x direction

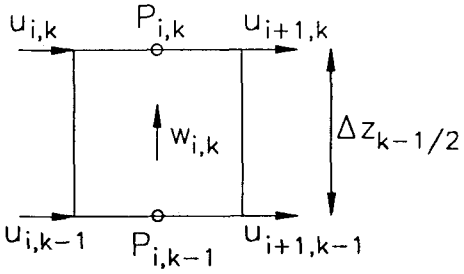

Figure 3. Volume Vol^z—momentum equation in the z direction

Now, the liquid momentum equation (13) in the z direction is integrated over the volume Vol^z shown in Figure 3:

$$Vol^z\left[(\alpha_\ell\rho_\ell)^n\frac{w_{\ell i,k}^{n+1}-w_{\ell i,k}^{n}}{\Delta t}+\alpha_\ell^n\frac{P_{i,k}^{n+1}-P_{i,k-1}^{n+1}}{\Delta z}-K_{g\ell}^n(w_{gi,k}^{n+1}-w_{\ell i,k}^{n+1})\right]$$
$$+\int_{Vol^z}C\cdot w_\ell\,dV=Vol^z(\alpha_\ell\rho_\ell)^n g_z \qquad (24)$$

and

$$d_\ell^z w_{\ell i,k}^{n+1}=a_\ell^z(P_{i,k}^{n+1}-P_{i,k-1}^{n+1})+b_\ell^z w_{gi,k}^{n+1}+c_\ell^z. \qquad (25)$$

The gas momentum equation (17) in the z direction is integrated over the volume Vol^z shown in Figure 3:

$$Vol^z\left[(\alpha_g\rho_g)^n\frac{w_{gi,k}^{n+1}-w_{gi,k}^{n}}{\Delta t}+\alpha_g^n\frac{P_{i,k}^{n+1}-P_{i,k-1}^{n+1}}{\Delta z}-K_{g\ell}^n(w_{\ell i,k}^{n+1}-w_{gi,k}^{n+1})\right]$$
$$+\int_{Vol^z}C\cdot w_g\,dV=Vol^z(\alpha_g\rho_g)^n g_z \qquad (26)$$

and

$$d_g^z w_{gi,k}^{n+1}=a_g^z(P_{i,k}^{n+1}-P_{i,k-1}^{n+1})+b_g^z w_{\ell i,k}^{n+1}+c_g^z. \qquad (27)$$

Now, the velocity of the other phase is eliminated in the discretized momentum equations. For the x direction,

$$u_{\ell i,k}^{n+1}=q_{\ell}^{x}(P_{i,k}^{n+1}-P_{i-1,k}^{n+1})+r_{\ell}^{x}, \tag{28}$$

$$u_{gi,k}^{n+1}=q_{g}^{x}(P_{i,k}^{n+1}-P_{i-1,k}^{n+1})+r_{g}^{x} \tag{29}$$

and for the z direction,

$$w_{\ell i,k}^{n+1}=q_{\ell}^{z}(P_{i,k}^{n+1}-P_{i,k-1}^{n+1})+r_{\ell}^{z} \tag{30}$$

$$w_{gi,k}^{n+1}=q_{g}^{z}(P_{i,k}^{n+1}-P_{i,k-1}^{n+1})+r_{g}^{z}. \tag{31}$$

Finally, the liquid mass conservation equation (18) is combined with the liquid momentum equations (28) and (30):

$$\mathrm{AE}_{\ell}P_{i+1,k}^{n+1}+\mathrm{AW}_{\ell}P_{i-1,k}^{n+1}+\mathrm{AN}_{\ell}P_{i,k+1}^{n+1}+\mathrm{AS}_{\ell}P_{i,k-1}^{n+1}-(\mathrm{AE}_{\ell}+\mathrm{AW}_{\ell}+\mathrm{AN}_{\ell}+\mathrm{AS}_{\ell})P_{i,k}^{n+1}$$
$$+\frac{\mathrm{Vol}^{\mathrm{m}}}{\Delta t}[(\alpha_{\ell}\rho_{\ell})_{i,k}^{n+1}-(\alpha_{\ell}\rho_{\ell})_{i,k}^{n}]=B_{\ell} \tag{32}$$

and the gas mass conservation equation (19) is combined with the gas momentum equations (29) and (31):

$$\mathrm{AE}_{g}P_{i+1,k}^{n+1}+\mathrm{AW}_{g}P_{i-1,k}^{n+1}+\mathrm{AN}_{g}P_{i,k+1}^{n+1}+\mathrm{AS}_{g}P_{i,k-1}^{n+1}-(\mathrm{AE}_{g}+\mathrm{AW}_{g}+\mathrm{AN}_{g}+\mathrm{AS}_{g})P_{i,k}^{n+1}$$
$$+\frac{\mathrm{Vol}^{\mathrm{m}}}{\Delta t}[(\alpha_{g}\rho_{g})_{i,k}^{n+1}-(\alpha_{g}\rho_{g})_{i,k}^{n}]=B_{g}. \tag{33}$$

Equation (32) may be represented by the function

$$M_{\ell}(P_{i+1,k}, P_{i-1,k}, P_{i,k-1}, P_{i,k}, \alpha_{\ell}\rho_{\ell})=0. \tag{34}$$

The equation ${}^{k+1}M_{\ell}^{n+1}=0$ may be solved by the Newton iterative method, i.e.

$${}^{k}M_{\ell}^{n+1}+\frac{\partial M_{\ell}}{\partial P_{i+1,k}}\delta P_{i+1,k}+\frac{\partial M_{\ell}}{\partial P_{i-1,k}}\delta P_{i-1,k}+\ldots+\frac{\partial M_{\ell}}{\partial P_{i,k}}\delta P_{i,k}+\frac{\partial M_{\ell}}{\partial \alpha_{\ell}}\delta\alpha_{\ell}=0. \tag{35}$$

Then

$$\mathrm{AE}_{\ell}\delta P_{i+1,k}+\mathrm{AW}_{\ell}\delta P_{i-1,k}+\mathrm{AN}_{\ell}\delta P_{i,k+1}+\mathrm{AS}_{\ell}\delta P_{i,k-1}$$
$$-\left(\mathrm{AE}_{\ell}+\mathrm{AW}_{\ell}+\mathrm{AN}_{\ell}+\mathrm{AS}_{\ell}-\frac{\mathrm{Vol}^{\mathrm{m}}}{\Delta t}\alpha_{\ell}\frac{\partial\rho_{\ell}}{\partial P}\right)\delta P_{i,k}+\frac{\mathrm{Vol}^{\mathrm{m}}}{\Delta t}\rho_{\ell}\delta\alpha_{\ell}=-{}^{k}M_{\ell}^{n+1}. \tag{36}$$

In the same way, equation (33) may be represented by the function

$$M_{g}(P_{i+1,k}, P_{i-1,k}, P_{i,k-1}, P_{i,k}, \alpha_{g}\rho_{g})=0. \tag{37}$$

Solving ${}^{k+1}M_{g}^{n+1}=0$ by the Newton iterative method

$${}^{k}M_{g}^{n+1}+\frac{\partial M_{g}}{\partial P_{i+1,k}}\delta P_{i+1,k}+\frac{\partial M_{g}}{\partial P_{i-1,k}}\delta P_{i-1,k}+\ldots+\frac{\partial M_{g}}{\partial P_{i,k}}\delta P_{i,k}+\frac{\partial M_{g}}{\partial \alpha_{g}}\delta\alpha_{g}=0. \tag{38}$$

Then

$$\mathrm{AE}_{g}\delta P_{i+1,k}+\mathrm{AW}_{g}\delta P_{i-1,k}+\mathrm{AN}_{g}\delta P_{i,k+1}+\mathrm{AS}_{g}\delta P_{i,k-1}$$
$$-\left(\mathrm{AE}_{g}+\mathrm{AW}_{g}+\mathrm{AN}_{g}+\mathrm{AS}_{g}-\frac{\mathrm{Vol}^{\mathrm{m}}}{\Delta t}\alpha_{g}\frac{\partial\rho_{g}}{\partial P}\right)\delta P_{i,k}+\frac{\mathrm{Vol}^{\mathrm{m}}}{\Delta t}\rho_{g}\delta\alpha_{g}=-{}^{k}M_{g}^{n+1}. \tag{39}$$

Equations (36) and (39) are combined to eliminate $\delta\alpha_k$:

$$\mathrm{AE}\,\delta P_{i+1,k}+\mathrm{AW}\,\delta P_{i-1,k}+\mathrm{AN}\,\delta P_{i,k+1}+\mathrm{AS}\,\delta P_{i,k-1}+\mathrm{A}\,P_{i,k}=\mathrm{SM}. \tag{40}$$

Equation (40) represents a system of N equations (N = number of cells) for the pressure at each cell as a function of the pressure in the neighbouring cells. This system of equations can be solved, e.g. by the tri-diagonal matrix algorithm.

Once the pressure field is known, the velocities are calculated from the momentum equations and the volumetric fractions are calculated from the mass conservation equations.

The convergence of the numerical method is obtained when

$$^{k+1}M_\ell=0 \quad \text{and} \quad ^{k+1}M_g=0, \tag{41}$$

and the mass conservation is obtained when

$$^{k}M_\ell=0 \quad \text{and} \quad ^{k}M_g=0. \tag{42}$$

The time increment per computational cycle δt is based on the maximum fluid speed of the system, u_m:

$$u_m\frac{\delta t}{\delta x}=f, \tag{43}$$

where δx is the smallest cell dimension and f is a specified number with magnitude somewhat less than unity. We have obtained satisfactory results using $f=0{\cdot}5$.

CONSTITUTIVE EQUATION

To solve the conservation equations of the two-fluid model presented above, we need to specify a constitutive equation for the interfacial momentum transfer term. There are at least two transient forces in addition to the interfacial friction force: the virtual mass and the Basselt force.[11] In this study we are mainly interested in the steady-state flow in the T-junction: then our attention is directed to the interfacial friction modelling.

The interfacial friction term has been modelled successfully for the dispersed two-phase flow.[11] By neglecting the lift force due to the rotation of the particles and the diffusion force due to the concentration gradient and for spherical particles, the interfacial friction coefficient $K_{g\ell}$ may be modelled[16] by a simple form such as

$$K_{g\ell}=\frac{3}{8}\frac{\alpha_d}{r_p}C_D\rho_c|V_r|, \tag{44}$$

where α_d is the volumetric fraction of the dispersed phase, r_p the particle radius, C_D the drag coefficient, ρ_c the density of the continuous phase and V_r is the relative velocity (V_g-V_ℓ).

For spherical particles the interfacial area concentration may be given by the following relation:

$$a_i=\frac{3\alpha_d}{r_p}. \tag{45}$$

Using the above relation the interfacial friction coefficient expression (44) may be rewritten as

$$K_{g\ell}=\tfrac{1}{8}a_iC_D\rho_c|V_r|. \tag{46}$$

The interfacial momentum transfer term is now expressed as a product of the interfacial area and the driving force, i.e. the friction force. This expression cannot be helpful unless the drag

Table I. Interfacial friction model. Values of C $(m-1)$

Flow No. 1	Flow No. 2	Flow No. 4	Flow No. 5	Flow No. 6	Average	Mean deviation
250	100	260	190	240	200	26%

coefficient and the interfacial area are known. The drag coefficient has been modelled[11] for different flow patterns, but it still remains valid only for dispersed flow. Many investigations have been carried out in the two-phase interfacial area,[17-19] but to date no general model is available.

The two-phase flow distribution in a T-junction generally shows a very complex interfacial structure with spatial distribution of the phases that is quite different from straight tube dispersed flows. Then the available models for the drag coefficient and the interfacial area cannot be used for an accurate numerical prediction of the phase distribution in the T-junction.

The interfacial friction coefficient (46) for the dispersed flow may be extended to a general form by using the mixture density instead of the continuous phase density:

$$K_{g\ell} = a_i C_D \rho_m |V_r|, \tag{47}$$

where the mixture density is given by

$$\rho_m = \alpha_g \rho_g + \alpha_\ell \rho_\ell. \tag{48}$$

The interfacial area and the drag coefficient in the above expression are supposed to be a function of the void fraction. The interfacial area must vanish when the volumetric fraction of one phase vanishes: then a general for the interfacial friction coefficient may be given by

$$K_{g\ell} = C \alpha_\ell \alpha_g \rho_m |V_r| \tag{49}$$

In a preliminary study[20] the above expression for the interfacial friction coefficient was used to simulate five experimental data points[2] for the two-phase flow separation in a T-junction. For each flow condition the outlet pressures are fixed to give the same mass split ratio ($W3/W1$), while the value of the constant C in expression (49) is adjusted to give the same phase separation ($x3/x1$). The resulting values of C are presented in Table I.

Using the average value for C in equation (49) we obtain the constitutive equation for the interfacial friction coefficient that will be used in the T-junction numerical simulations:

$$K_{g\ell} = 200\ \alpha_\ell \alpha_g \rho_m |V_r|. \tag{50}$$

DISCUSSION OF RESULTS

The constitutive equation (50) for the interfacial friction coefficient developed above was introduced in the TOFLU-2D computer code. A set of 17 experimental data points for the two-phase flow in a vertical T-junction was used to test the ability of the code to predict the observed phase separation.

Two different numerical grids are used for the flow simulation in the T-junction. A 10×15 grid shown in Figure 4(a) was used for most of the simulations. An extended 15×20 grid shown in Figure 4(b) was used to investigate the influence of the outlet boundary conditions.

For the inlet boundary conditions, it is necessary to specify the liquid and the gas velocities and the void fraction. These values are calculated from the experimental data by using the homogeneous

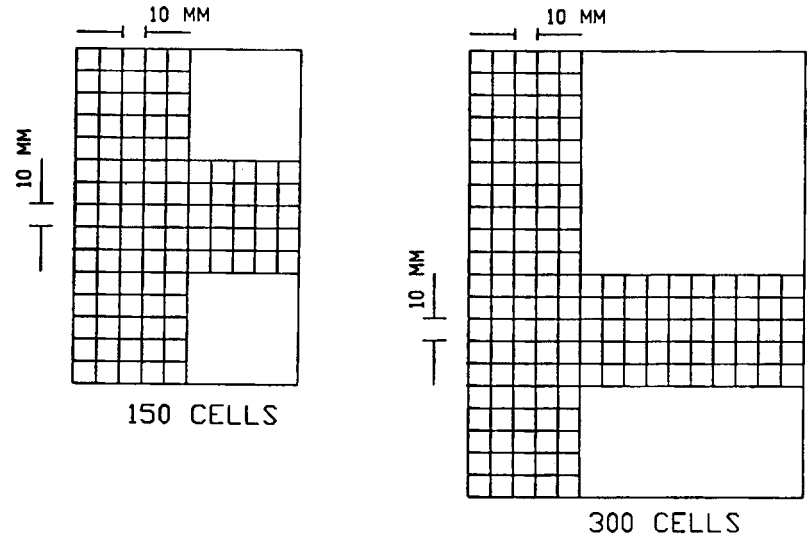

Figure 4. Numerical grids (a) NX × NZ = 10 × 15; (b) NX × NZ = 15 × 20

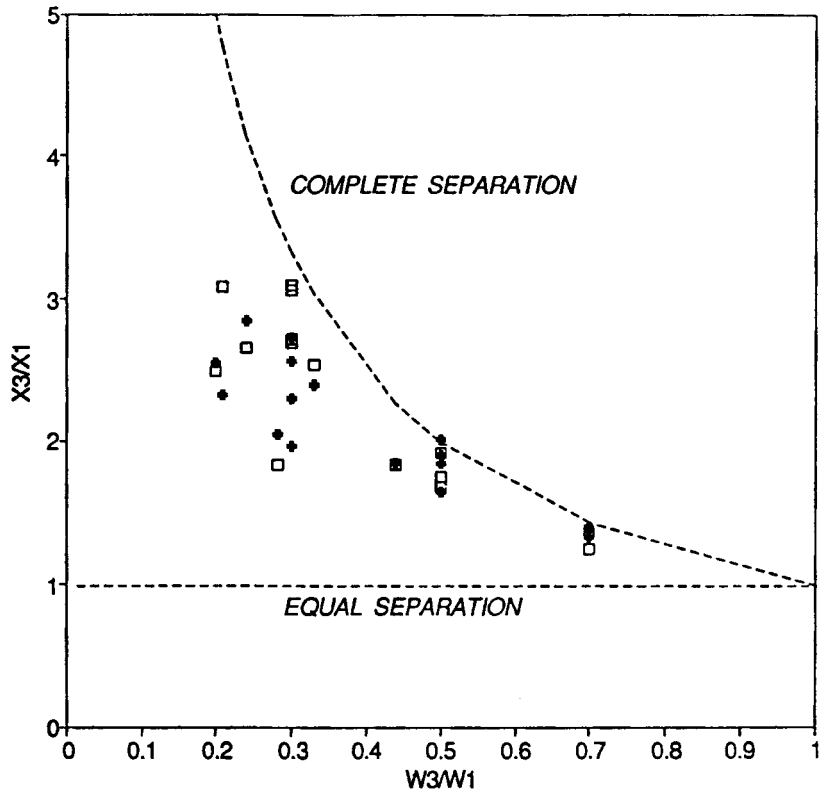

Figure 5. Phase separation in the T-junction (+experimental data,[2,9] □ prediction)

relations:

$$V_\ell = V_g = V_{s\ell} + V_{sg}, \tag{51}$$

$$\alpha = \frac{1}{(1 + V_{s\ell}/V_{sg})}, \tag{52}$$

where $V_{s\ell}$ is the liquid superficial velocity and V_{sg} is the gas superficial velocity.

The outlet pressures are specified as the outlet boundary conditions. The branch pressure ($P3$) is maintained constant and the main outlet pressure ($P2$) is changed by small steps in order to obtain different values for the mass split ratio ($W3/W1$), where $W3$ is the total mass flow rate in the branch and $W1$ is the total mass flow rate at the inlet of the T-junction.

The predicted phase separation obtained from the numerical results are compared with the experimental data[2,9] in Figures 5 and 6. Figure 5 shows the experimental and numerical values of the phase separation ratio ($x3/x1$) as a function of the mass split ratio ($W3/W1$). A comparison between the calculated and the measured value of the phase separation ratio is shown in Figure 6. It can be seen in this figure that 90% of the experimental data is predicted within $\pm 20\%$. The mean deviation for all the data set is about 9%. A good agreement is found for high mass split ratio data, for which the phase separation ratio is near to the complete separation line. However, for low values of the mass split ratio some experimental points are under-predicted.

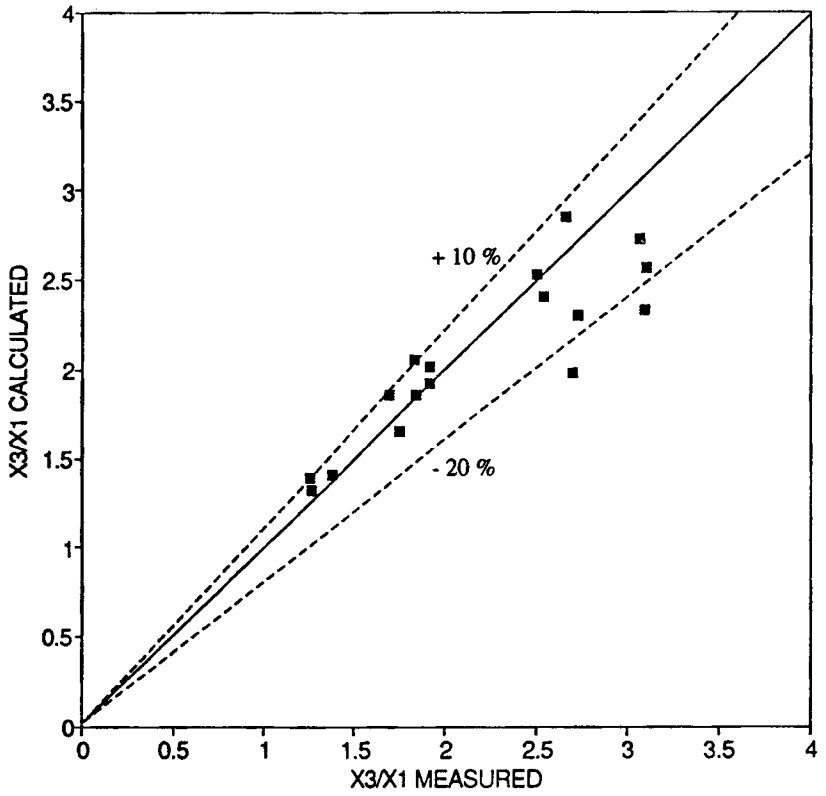

Figure 6. Phase separation in the T-junction

In a recent work about the two-phase flow distribution phenomena Lahey[21] concluded that the two-dimensional simulation cannot predict accurately the low mass split ratio results. Under such a condition only a three-dimensional numerical model can take into account the two-phase flow distribution in the real geometry of a circular T-junction.

The influence of the outlet boundary conditions was investigated by using the extended 15×20 grid shown in Figure 4(b). Now the outlet pressures are imposed at cross sections located two diameters upstream from the junction. The numerical results obtained with the extended grid are more accurate, principally for high mass split ratios. For these flow conditions, the pressure profiles near to the junction are not uniform and a constant pressure boundary condition imposed too close to the junction changes the flow distribution and the phase separation.

The phase distribution in the T-junction for $W3/W1 = 0{\cdot}50$ and $x3/x1 = 1{\cdot}91$ is shown in Figures 7–10. For this run the inlet mixture velocity is equal to 10·45 m/s and the inlet void fraction is equal to 0·81 ($V_{sl} = 2{\cdot}01$ m/s and $V_{sg} = 8{\cdot}44$ m/s). The flow pattern at the inlet is expected to be churn-turbulent.

The void fraction distribution is plotted in Figure 7. It can be observed that in the immediate vicinity of the junction most of the liquid phase is concentrated in the upper part of the branch and in the right-hand side of the main outlet, while the gas phase is concentrated in the centre and in the lower part of the branch. Figure 8 shows the pressure distribution. For this run the pressure

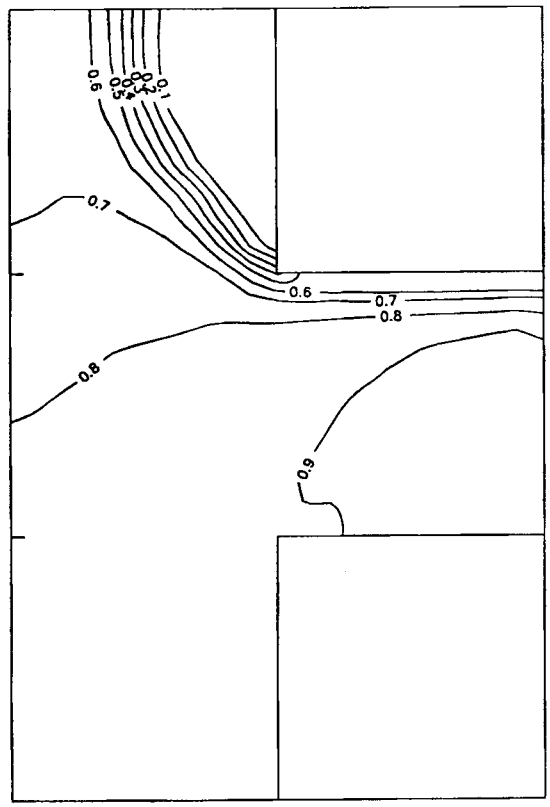

Figure 7. Void fraction distribution

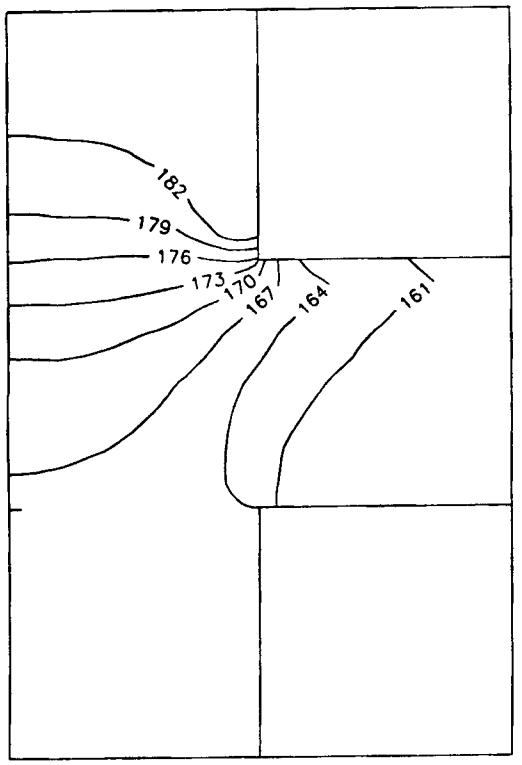

Figure 8. Pressure distribution (kPa)

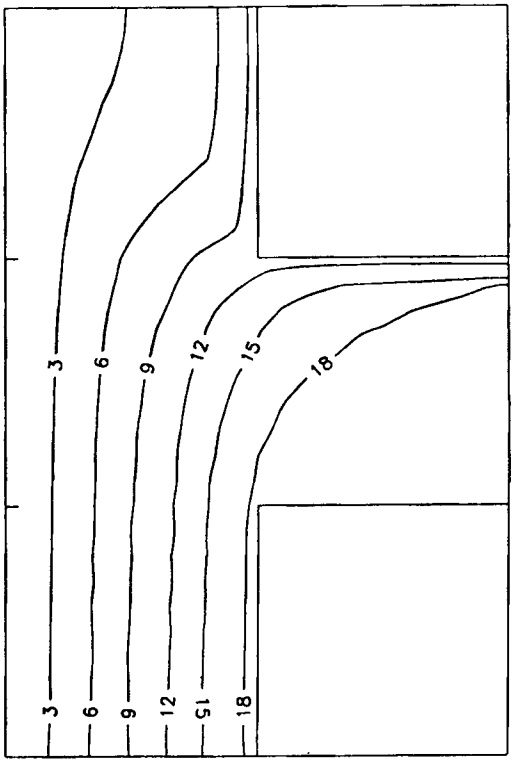

Figure 9. Liquid streamlines

boundary condition for the main outlet and the branch is set at 183·5 and 160·0 kPa, respectively. With respect to the inlet pressure, the pressure increases in the main tube and decreases in the branch tube.

The liquid and the gas streamlines are plotted in Figures 9 and 10, respectively. These streamlines represent the volumetric flow rate distribution in the T-junction and may be different from the liquid and gas particles trajectory because of the void fraction field. A uniform flow distribution of the gas phase is observed in the branch while the liquid phase is split in the junction creating a high liquid concentration region in the top of the branch and the right-hand side of the main tube.

CONCLUSIONS

It has been shown that the two-dimensional two-fluid computer code TOFLU-2D is able to predict the phase separation in a T-junction. The numerical technique developed in this paper is very stable and converges after a few iterations. A general constitutive equation for the interfacial friction coefficient was developed to simulate the T-junction two-phase flow.

The predicted phase separation ratio ($x3/x1$) agrees quite well with the experimental data for a vertical T-junction air-water flow. The prediction accuracy ($\pm 20\%$) is found to be compatible with a two-dimensional code. Some experimental phase separation data are under-predicted showing that in some cases a three-dimensional model would be more suitable.

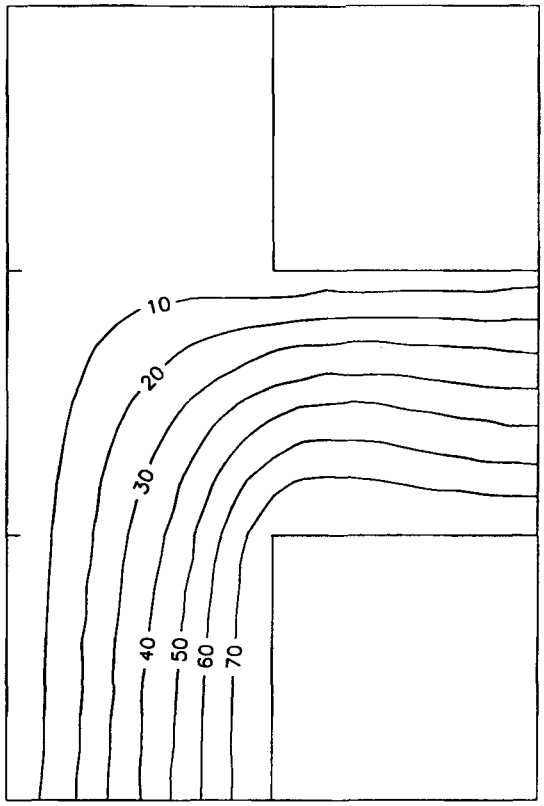

Figure 10. Gas streamlines

These results showed the ability of the two-fluid model to simulate the two-phase distribution, but further research is needed to improve the simulation accuracy. In particular more research is needed in the modelling of the interfacial area concentration and the drag coefficient in two-phase flows.

REFERENCES

1. B. J. Azzopardi, 'Measurements and observation of the split of annular flow at a vertical T-junction', *Int. J. Multiphase Flow*, **14**, 701–710 (1988).
2. M. R. Davis and B. Fungtamasan, 'Two-phase flow through pipe branch junctions'. *Int. J. Multiphase Flow*, **16**, 799–817 (1990).
3. S. T. Hwang, H. M. Soliman and R. T. Lahey, Jr., 'Phase separation in dividing two-phase flows', *Int. J. Multiphase Flow*, **14**, 439–458 (1988).
4. R. T. Lahey, Jr., 'Current understanding of phase separation mechanisms in branching conduits', *Nucl. Eng. Design*, **95**, 145–161 (1986).
5. G. E. McCrerry and S. Banerjee, 'Phase separation of dispersed mist and dispersed annular (rivulet or thin film) flow in a tee-Part I: experiments', *Int. J. Multiphase Flow*, **16**, 429–446 (1990).
6. G. E. McCrerry and S. Banerjee, 'Phase separation of dispersed mist and dispersed annular (rivulet or thin film) flow in a tee-Part II: analysis', *Int. J. Multiphase Flow*, **17**, 309–325 (1991).
7. M. T. Rubel, H. M. Soliman and G. E. Sims, 'Phase distribution during steam–water flow in a horizontal T-junction, *Int. J. Multiphase Flow*, **14**, 425–438 (1988).
8. O. Shoham, J. P. Brill and Y. Taitel, 'Two-phase flow splitting in a tee junction: experimental and modelling', *Chem. Eng. Sci.*, **42**, 2667–2676 (1987).

9. T. J. Honan and R. T. Lahey, Jr., 'The measurement of phase separation in wyes and tees', *Nucl. Eng. Design*, **64**, 93–102 (1981).
10. R. T. Lahey, Jr. and D. A. Drew, 'The current state-of-the-art in the modelling of vapor/liquid two-phase flows', *Proc. ASME Winter Annu. Meet.*, Dallas, 25–30 November 1990.
11. M. Ishii and K. Mishima, 'Two-fluid model and hydrodynamic constitutive relations', *Nucl. Eng. Design*, **82**, 107–126 (1984).
12. H. B. Stewart and B. Wendroff, 'Two-phase flow: models and methods', *J. Comput. Phys.*, **56**, 363–409 (1984).
13. M. Ishii, *Thermo-Fluid Dynamic Theory Of Two-Phase Flows*, Eyrolles, Paris, 1975.
14. S. V. Patankar, *Numerical Heat Transfer And Fluid Flow*, McGraw-Hill, New York, 1980.
15. L. F. M. Moura and K. Rezkallah, 'TOFLU-2D: a two-dimensional two-fluid computer code', *Tech. Rep. No. MRG-91-1*, University of Saskatchewan, Canada, 1991.
16. M. Ishii and N. Zuber, 'Drag coefficient and relative velocity in bubbly, droplet or particulate flows', *AIChE J.*, **25**, 843–855 (1979).
17. M. Ishii and K. Mishima, 'Study of two-fluid model and interfacial area', *Argonne National Laboratory Report ANL-80-111* (1980).
18. J. M. DeJesus and M. Kawaji, 'Measurement of interfacial area and void fraction in upward, cocurrent gas–liquid flow', *Proc. ANS National Heat Transfer Conf.*, U.S.A., 1989.
19. J. M. Delhaye and P. Bricard, 'Interfacial area in bubbly flow: experimental data and correlations', *Proc. ANS National Heat Transfer Conf.*, U.S.A. (1991).
20. L. F. M. Moura and K. Rezkallah, 'Numerical simulation of two-phase gas–liquid flows', *Tech. Report No. MRG-91-2*, University of Saskatchewan, Canada, 1991.
21. R. T. Lahey, Jr., 'The analysis of the phase separation and the phase distribution phenomena using two-fluid models', *Nucl. Eng. Design* **122**, 17–40 (1990).